MACULAR DEGENERATION

Targeting factor D of the alternative complement pathway reduces geographic atrophy progression secondary to age-related macular degeneration

Brian L. Yaspan,[1] David F. Williams,[2] Frank G. Holz,[3] Carl D. Regillo,[4] Zhengrong Li,[1] Amy Dressen,[1] Menno van Lookeren Campagne,[1] Kha N. Le,[1] Robert R. Graham,[1] Tatiana Beres,[1] Tushar R. Bhangale,[1] Lee A. Honigberg,[1] Ashley Smith,[1] Erin C. Henry,[1] Carole Ho,[1] Erich C. Strauss;[1]* for the MAHALO Study Investigators†

Geographic atrophy is an advanced form of age-related macular degeneration (AMD) and a leading cause of vision loss for which there are no approved treatments. Genetic studies in AMD patients have implicated dysregulation of the alternative complement pathway in the pathogenesis of geographic atrophy. Lampalizumab is a potential therapeutic that targets complement factor D, a pivotal activator of the alternative complement pathway. The MAHALO phase 2 clinical trial was a multicenter, randomized, controlled study that evaluated lampalizumab administered by intravitreal injection monthly (n = 42) and every other month (n = 41) versus sham control (n = 40) in patients with geographic atrophy secondary to AMD. The primary endpoint was the mean change in lesion area from baseline to month 18 as measured by fundus autofluorescence. Specific AMD-associated genetic polymorphisms were also analyzed. The MAHALO study met its primary efficacy endpoint with an acceptable safety profile; monthly lampalizumab treatment demonstrated a 20% reduction in lesion area progression versus sham control [80% confidence interval (CI), 4 to 37%]. A more substantial monthly treatment benefit of 44% reduction in geographic atrophy area progression versus sham control (95% CI, 15 to 73%) was observed in a subgroup of complement factor I (*CFI*) risk-allele carriers (57% of the patients analyzed were *CFI* risk-allele carriers). The MAHALO study shows a potential treatment effect in patients with geographic atrophy and supports therapeutic targeting of the alternative complement pathway for treating AMD pathogenesis.

INTRODUCTION

Age-related macular degeneration (AMD) is the leading cause of irreversible and profound visual impairment in industrialized countries (*1*). Advanced AMD is distinguished by either neovascular disease or geographic atrophy. The majority of severe vision loss in advanced disease has been associated with neovascular AMD; however, with the advent of available treatments for this form of the disease, geographic atrophy-related visual impairment is increasing relative to neovascular AMD. Geographic atrophy affects more than 5 million patients worldwide, and it is associated with devastating effects on visual function that affect the quality of life (*2*, *3*). Geographic atrophy is characterized by irreversible visual impairment resulting from loss of photoreceptors, retinal pigment epithelium, and the choriocapillaris. Geographic atrophy represents a significant unmet medical need because there are no approved or effective therapies to prevent progression of the disease and associated visual loss (*4*).

AMD is a multifactorial disease with genetic and environmental risk factors (*5*). Preclinical modeling of human AMD presents significant challenges, including replicating advanced age, complex genetic risk factors, and decades of environmental exposures that may contribute to the development and progression of geographic atrophy (*6*). Moreover, murine models have limitations because they lack the specialized human macular anatomy involved in AMD. Although mouse models have been used to study various aspects of AMD, currently there is no preclinical model that approximates the pathological spectrum of geographic atrophy. Consequently, identifying potential therapeutic targets for treating geographic atrophy has focused on human genetic studies. Although the precise pathogenesis of AMD remains to be determined, it is well established that there is a major genetic contribution to disease risk. Several studies have demonstrated that polymorphisms in loci containing genes coding for proteins in the alternative complement pathway are strongly associated with the risk of developing AMD, including the advanced forms of the disease. Confirmed AMD common risk loci include genes encoding complement factor H (CFH), complement factor I (CFI), complement component 3 (C3), and one locus containing complement component 2 (C2) and complement factor B (CFB) designated as C2/CFB (*7*, *8*). With the exception of C2, all of these complement components are primarily associated with the alternative complement pathway (*9*). Moreover, dysregulation of the complement system, particularly the alternative complement pathway, has been implicated in the pathogenesis of AMD (*4*, *10*). Furthermore, recent studies have shown increased concentrations of complement proteins in the serum of AMD patients compared to controls, including complement factor D (CFD) (*11*, *12*), a pivotal regulator of the alternative complement pathway. CFD acts early in the alternative complement pathway, is a rate-limiting enzyme of the pathway, and is present at relatively low plasma concentrations compared to other complement factors (*13*). For these reasons, we considered CFD as a potential therapeutic target in the alternative complement pathway for treating geographic atrophy. Lampalizumab, previously referred to as FCFD4514S and anti–factor D, is an antigen-binding fragment (Fab) of a humanized monoclonal antibody (mAb) directed against CFD (*14*). Lampalizumab selectively inhibits CFD-mediated activation and amplification of the alternative complement pathway, but it does not affect initiation of

[1]Genentech Inc., South San Francisco, CA 94080, USA. [2]VitreoRetinal Surgery, PA, Minneapolis, MN 55404, USA. [3]Department of Ophthalmology, University of Bonn, Bonn, Germany. [4]Wills Eye Hospital, Philadelphia, PA 19107, USA.
*Corresponding author. Email: strauss.erich@gene.com
†MAHALO study investigators are listed in the Acknowledgments.

the classical or mannose-binding lectin pathways of the complement system (*9*, *15*, *16*).

The MAHALO phase 2 clinical trial [ClinicalTrials.gov identifier, NCT01229215; EudraCT (European Union Drug Regulating Authorities Clinical Trials) number, 2010-019183-36] investigated the safety, tolerability, pharmacokinetics, and evidence of activity of lampalizumab, including targeted genetic analyses, in patients with geographic atrophy secondary to AMD.

RESULTS

Study design and patient characteristics

The MAHALO phase 2 clinical trial enrolled 129 eligible patients (Fig. 1). Patients were randomized 1:2:1:2 to sham monthly, 10-mg lampalizumab monthly, sham every other month, or 10-mg lampalizumab every other month; the 10-mg dose of lampalizumab was in a 100-µl volume administered by intravitreal injection. One hundred and twenty-three patients met the prespecified criteria for analyses. Prespecified analysis criteria required that patients received at least one dose of treatment and had at least one post-baseline fundus autofluorescence measurement of the geographic atrophy area. Study arms were balanced for demographic and ocular characteristics (Table 1). Before the month 18 endpoint, there were 30 discontinuations: 19 were due to patient or physician decisions (for example, related to comorbidities: Alzheimer's disease, osteoarthritis, prostate cancer, Crohn's disease, and aortic aneurysm), 9 were due to reported adverse events, and 2 were related to a condition that required another therapeutic intervention [conversion to neovascular AMD requiring anti–vascular endothelial growth factor (VEGF) treatment]. Although there was a numerically higher percentage of discontinuations in the lampalizumab treatment groups versus the pooled sham group, the overall range of dropout time among the three treatment groups was predominantly overlapping (fig. S1). Moreover, the onset of the treatment effect observed in the lampalizumab monthly group at month 6 occurred when dropout rates and timing were very similar across the treatment groups. There were no apparent differences or patterns for discontinuations across the treatment groups.

Clinical, genetic, and pharmacokinetic analyses

The primary efficacy outcome measure was the mean change in geographic atrophy area from baseline to month 18 assessed by fundus

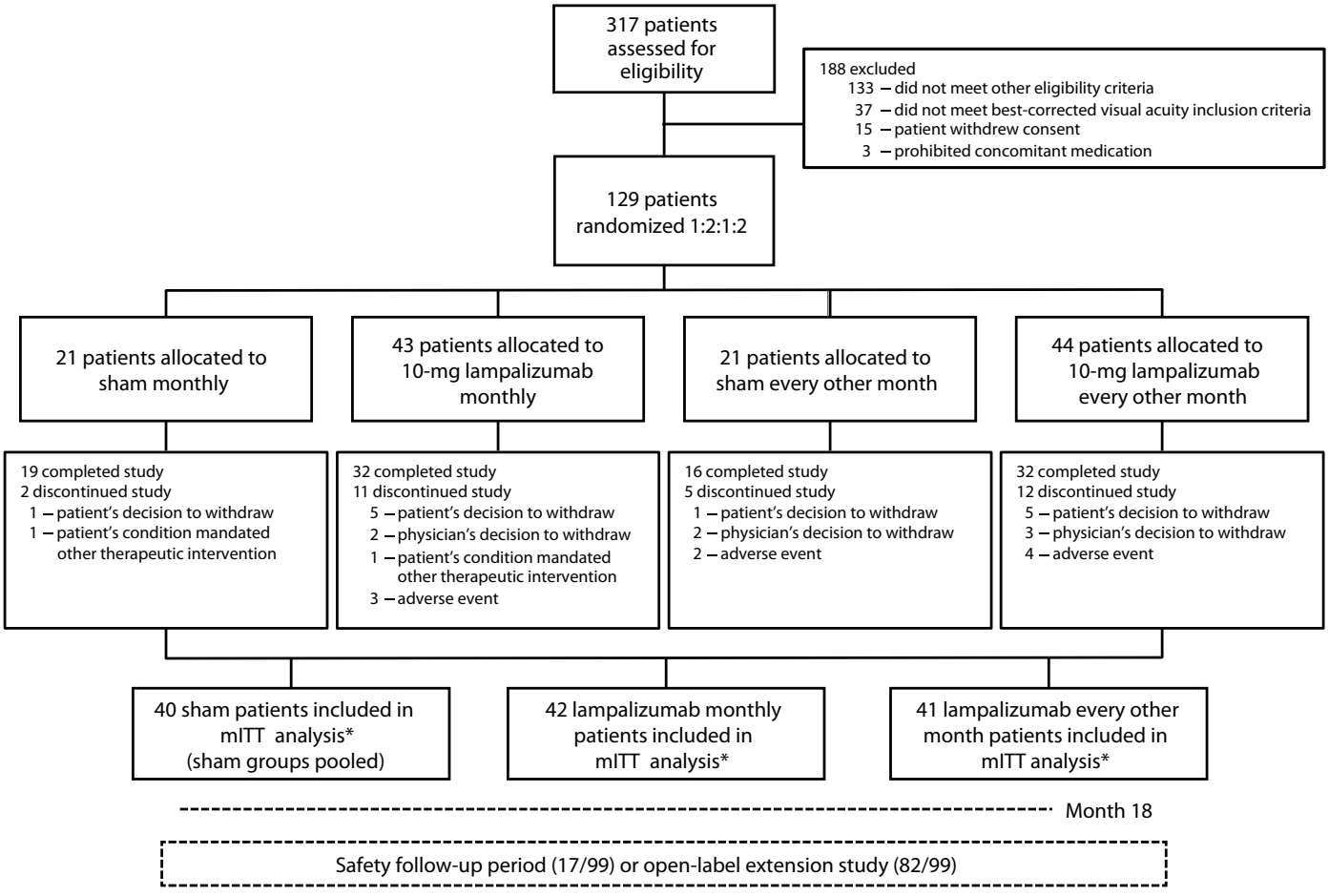

Fig. 1. MAHALO clinical trial flowchart. This was a phase 2, multicenter, randomized, controlled study that investigated the safety, tolerability, pharmacokinetics, and evidence of activity of lampalizumab in patients with geographic atrophy secondary to AMD. One hundred twenty-nine eligible patients were randomized 1:2:1:2 to sham monthly, 10-mg lampalizumab monthly, sham every other month, or 10-mg lampalizumab every other month. *One hundred twenty-three patients met the prespecified modified intention-to-treat (mITT) criteria for primary efficacy analysis. This population included all randomized patients who had one or more treatment injections and one or more post-baseline geographic atrophy measurements. Sham arms were pooled for analyses.

Table 1. Baseline characteristics of individual cohorts and all mITT patients. EOM, every other month; BCVA, best-corrected visual acuity; DA, disc area (1 DA = 2.54 mm^2); GA, geographic atrophy.

	Sham pooled (*n* = 40)	Lampalizumab monthly (*n* = 42)	Lampalizumab EOM (*n* = 41)	All mITT patients (*n* = 123)
Patient demographics				
Age (years), mean (SD)	78.5 (7.3)	80.4 (7.2)	77.2 (7.3)	78.7 (7.3)
Sex (female), *n* (%)	24 (60.0)	28 (66.7)	18 (43.9)	70 (56.9)
Race (white), *n* (%)	40 (100.0)	40 (95.2)	41 (100.0)	121 (98.4)
Study eye characteristics				
BCVA letters, mean (SD)	45.9 (13.4)	47.6 (12.8)	49.5 (11.0)	47.7 (12.4)
Snellen equivalent (median)	20/125	20/100	20/100	20/100
Total area of GA, DA (SD)	3.48 (1.65)	3.37 (1.52)	3.37 (1.93)	3.41 (1.69)
Total area of GA, mm^2 (SD)	8.85 (4.18)	8.56 (3.86)	8.56 (4.90)	8.65 (4.30)

autofluorescence. Geographic atrophy may result in severe, irreversible visual function deficits; however, the decline in vision with disease progression may be variable depending on the location of the geographic atrophy lesion. As a result, geographic atrophy lesion area and progression may not correlate well with central vision loss. Therefore, the quantitative measurement of geographic atrophy area progression by fundus autofluorescence imaging has become an acceptable primary endpoint for clinical studies.

In the primary analysis study population (mITT all-comer), the adjusted mean change (that is, least-squares mean change adjusted for baseline geographic atrophy area) from baseline to month 18 was 2.9 mm^2 in the pooled sham group, 2.3 mm^2 in the lampalizumab monthly group, and 3.1 mm^2 in the lampalizumab every other month group (Fig. 2A and table S1); the unadjusted mean change from baseline to month 18 was similar: 2.9, 2.2, and 3.1 mm^2 in the corresponding treatment groups, respectively (table S1). Compared with growth of the geographic atrophy area in the pooled sham group, the reduction in geographic atrophy area growth was 0.6 mm^2 [80% confidence interval (CI), 0.1 to 1.1] for the lampalizumab monthly group and −0.2 mm^2 (80% CI, −0.7 to 0.3) for the lampalizumab every other month group (table S1). The lampalizumab monthly arm showed a 20% reduction in mean change in geographic atrophy area progression relative to the pooled sham group at month 18 (Fig. 2A). The 20% reduction in the monthly arm (80% CI, 4 to 37%; $P = 0.117$) met the prespecified significance level ($P < 0.2$) for the MAHALO phase 2 study. The prespecified significance level in the MAHALO phase 2 was selected given that this was a proof-of-concept, hypothesis-generating clinical study with smaller sample size designed to identify minimal treatment efficacy that would be investigated in confirmatory phase 3 studies (*17*, *18*). Efficacy in the monthly lampalizumab arm was observed as early as month 6 and continued for the duration of the 18-month study. In the primary analysis, there was no apparent treatment benefit observed in the lampalizumab every other month arm as compared with the pooled sham control group. An evaluation of the lampalizumab treatment response and geographic atrophy area progression from baseline to month 18 was also performed in the primary analysis population based on stratification of baseline geographic atrophy lesion area: <4 disc areas (<10 mm^2) versus ≥4 disc areas (≥10 mm^2) (a disc area is an anatomic metric equivalent to approximately 2.5 mm^2). At month 18 relative to the sham control group, the treatment effect of monthly lampalizumab was similar between these two subgroups [0.511 mm^2 (80% CI, −0.069 to 1.092) in the subgroup of <4 disc areas versus 0.536 mm^2 (80% CI, −0.313 to 1.385) in the subgroup of ≥4 disc areas]; these results showed that monthly lampalizumab treatment reduced geographic atrophy area progression regardless of baseline lesion size.

As a secondary endpoint and an independent imaging assessment, color fundus photography was used to evaluate the mean change in geographic atrophy area from baseline to month 18. The adjusted mean area change from baseline to month 18 was 2.8 mm^2 in the pooled sham group, 2.2 mm^2 in the lampalizumab monthly group, and 2.7 mm^2 in the lampalizumab every other month group (table S1); the unadjusted mean change from baseline to month 18 was 2.8, 2.1, and 2.6 mm^2 in the pooled sham group, lampalizumab monthly group, and lampalizumab every other month group, respectively (table S1). The results of color fundus photography were consistent with the primary efficacy outcome with fundus autofluorescence. Best-corrected visual acuity was also included as a secondary outcome measure with the objective to evaluate the safety of lampalizumab versus sham treatment on visual acuity; best-corrected visual acuity is a test using standardized and optimal methods to measure visual function in clinical trials. The mean change from baseline in best-corrected visual acuity at month 18 was −4.9 letters (80% CI, −7.3 to −2.4) for the pooled sham group, −3.3 letters (80% CI, −5.7 to −0.9) for the monthly lampalizumab group, and −1.4 letters (80% CI, −3.8 to 1.1) for the every other month lampalizumab group (Fig. 2B and table S2). The best-corrected visual acuity results showed no safety concerns with lampalizumab treatment relative to the sham control.

Targeted genetic analyses and clinical subgroup outcomes

We hypothesized that common variants within the alternative complement pathway may affect geographic atrophy progression and lampalizumab treatment response. We performed a targeted, exploratory genetic analysis to assess this possibility. To limit the multiple testing burden, we selected four single-nucleotide polymorphisms (SNPs) in loci containing complement genes: *CFH*, *C2/CFB*, *CFI*, and *C3*. The selected SNP from each locus (*CFH*, rs1329428; *C2/CFB*, rs429608;

CFI, rs17440077; and *C3*, rs2230199) represented the variant, or best available proxy, most associated by *P* value assessment with AMD risk from a recent genetic meta-analysis by the AMD Gene Consortium (*8*). Because of sample size considerations, risk-allele heterozygotes and homozygotes were combined into one group and designated as risk-allele carriers. An assessment of geographic atrophy progression and treatment effect at the *CFH* and *C2/CFB* loci was precluded by the high prevalence of risk-allele carriers, 96% at the *CFH* and 98% at the *C2/CFB* loci. The prevalence of these risk alleles in the MAHALO study is consistent with other reports of risk-allele frequency in bilateral geographic atrophy cases (*6*) (table S3). An analysis of the *C3* risk allele did not reveal an association with disease progression or treatment response (table S4). However, in carriers of the *CFI* risk allele, we observed a potential association with geographic atrophy progression and a significant association (P = 0.0037) with lampalizumab treatment response (table S4). Of the patients assayed in the MAHALO study, 57% were carriers of the common CFI risk allele.

To assess disease progression based on *CFI* genotype, geographic atrophy area was measured by fundus autofluorescence in risk-allele carriers and compared with noncarriers in the pooled sham group. In sham-treated *CFI* risk-allele carriers, a numerical increase of 49% in geographic atrophy area progression at month 18 was observed as compared with the sham-treated *CFI* risk-negative subgroup (Fig. 3 and table S5). However, the study was not powered to detect a difference in geographic atrophy area between the *CFI* risk-allele carrier group and the *CFI* risk-negative sham group. Given the relatively small sample size of the MAHALO phase 2 study, this numerical trend between *CFI* risk-allele carrier and *CFI* risk-negative subgroups will require further investigation in the ongoing phase 3 trials. The *CFI* genotype was also evaluated for a potential association with lampalizumab treatment response. For *CFI* risk-allele carriers, there was a 44% reduction in geographic atrophy area progression at month 18 in the monthly lampalizumab-treated subgroup relative to the *CFI* pooled sham subgroup (95% CI, 15 to 73%; P = 0.0037) (Fig. 4A and table S5); representative fundus autofluorescence images are shown in Fig. 4B. However, there was no apparent lampalizumab treatment effect in *CFI* risk-negative patients (Fig. 4C and table S5). On the basis of the mixed-effect model with baseline geographic atrophy area as a continuous variable, time point as a categorical variable, treatment, time-by-treatment interaction, treatment-by-*CFI* status, and baseline geographic atrophy category (≥10 mm^2 versus <10 mm^2), the test of treatment-by-*CFI* interaction showed a P value of 0.014, suggesting an outcome consistent with a potential predictive marker. Moreover, the *CFI* subgroup analysis suggested that the 20% reduction in geographic atrophy area observed in the monthly lampalizumab all-comer analysis (Fig. 2A) was driven exclusively by the 44% reduction in geographic atrophy area in the *CFI* risk-allele carrier subgroup (Fig. 4, A and C).

Next, we analyzed the *CFI* genotype in the every other month subgroups. In the *CFI* risk-allele carrier subgroup treated with lampalizumab

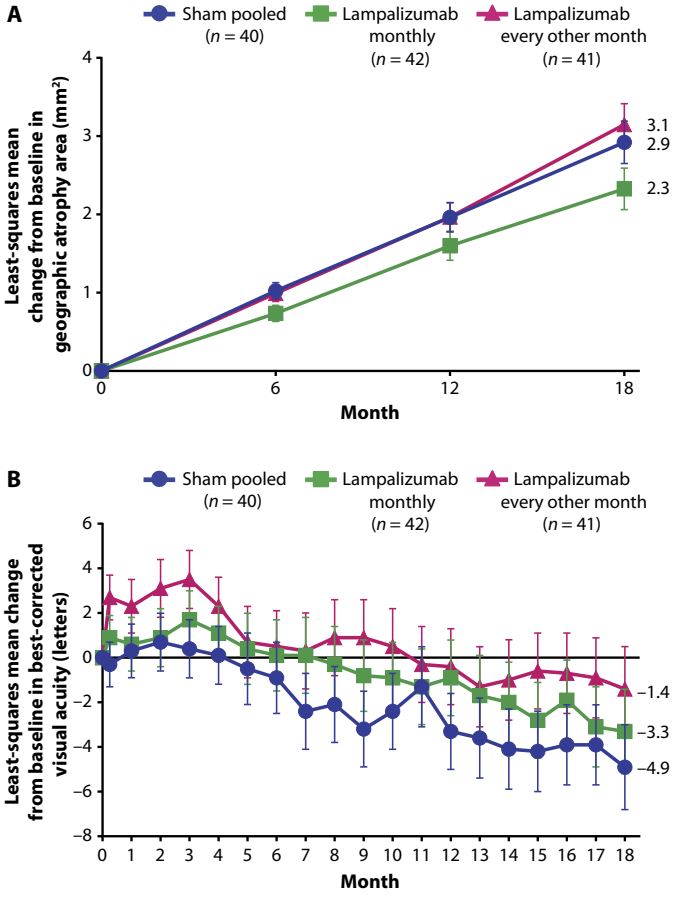

Fig. 2. Changes in geographic atrophy area and best-corrected visual acuity after lampalizumab treatment. Shown are mean changes from baseline to month 18 in geographic atrophy area by fundus autofluorescence (**A**) and in best-corrected visual acuity (**B**) based on the mITT population. (A) The lampalizumab monthly arm showed a 20% reduction in mean change in geographic atrophy area progression relative to the pooled sham group at month 18; this result met the prespecified significance level (P < 0.2) for the study. (B) The best-corrected visual acuity results showed no safety concerns with lampalizumab treatment relative to the sham control. Adjusted mean in (A) and (B) is the least-squares mean from the stratified analysis of variance (ANOVA) model adjusted for baseline geographic atrophy and baseline best-corrected visual acuity, respectively, using last observation carried forward (LOCF) data. Vertical bars are ±1 SE of the least-squares mean.

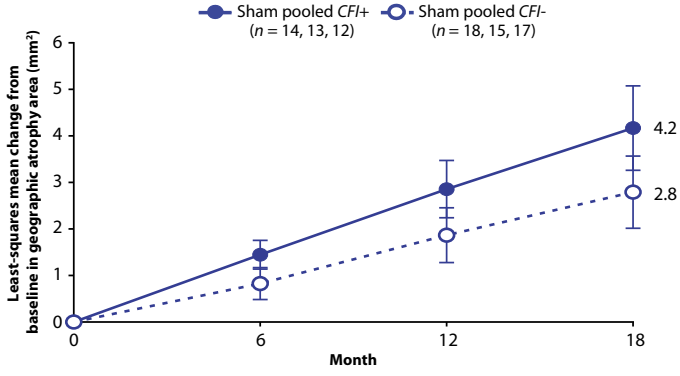

Fig. 3. Differential geographic atrophy area progression by fundus autofluorescence in the *CFI*+ (risk-allele carriers) versus *CFI*– (risk-negative) sham treatment subgroups. In sham-treated *CFI* risk-allele carriers, a numerical increase of 49% in geographic atrophy area progression at month 18 was observed as compared with the sham-treated *CFI* risk-negative subgroup. The least-squares mean was estimated from a linear mixed-effect model that included baseline geographic atrophy area as a continuous variable, time point as a categorical variable, treatment, time-by-treatment interaction, and baseline geographic atrophy category (≥10 mm^2 versus <10 mm^2). Vertical bars are 95% CIs of the least-squares mean. In parentheses, *n* corresponds to the number of patients at the 6-, 12-, and 18-month time points, respectively.

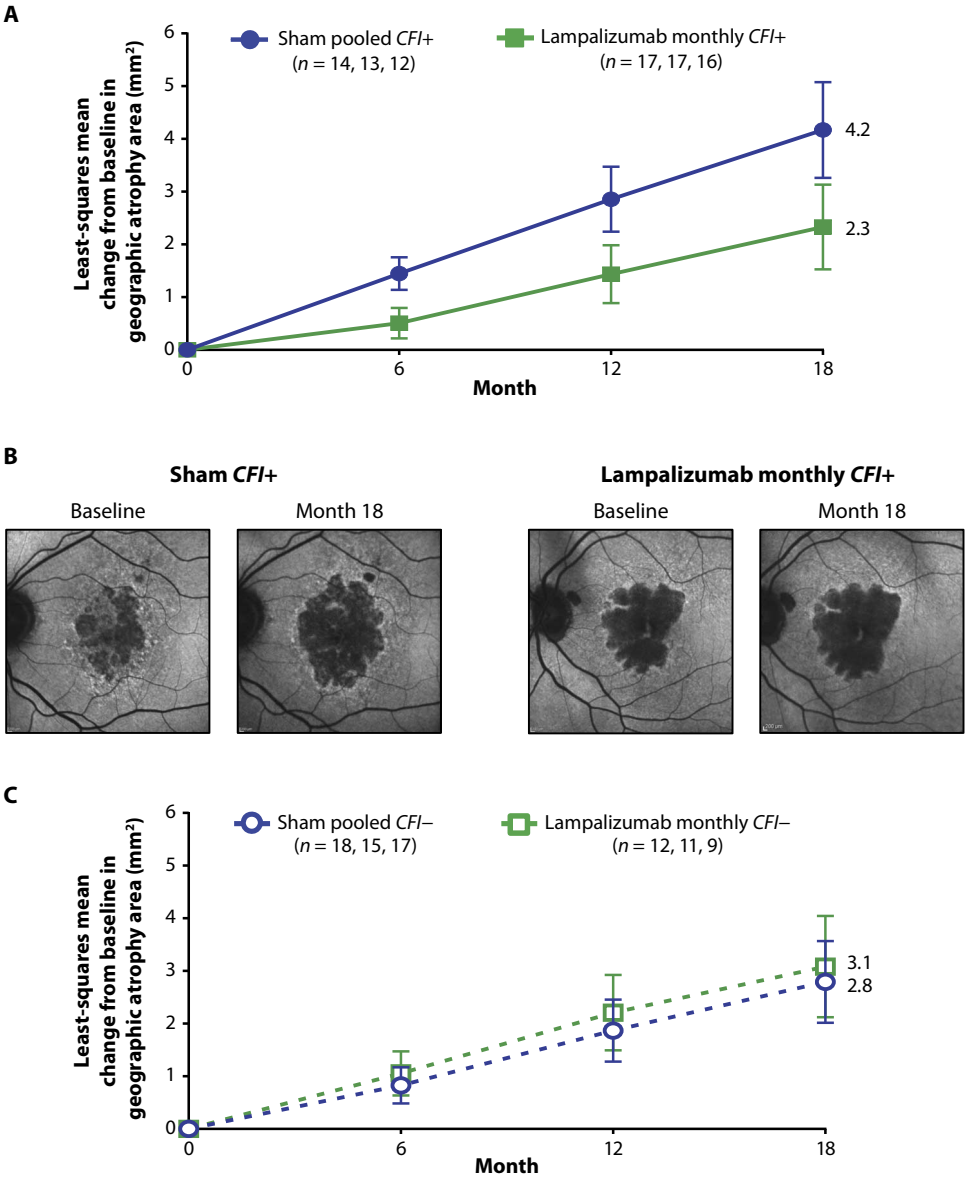

Fig. 4. Geographic atrophy progression in *CFI* risk-allele carriers and risk-negative subpopulations after monthly lampalizumab treatment. Shown is geographic atrophy progression by fundus autofluorescence in the *CFI*+ (risk-allele carriers) and *CFI*– (risk-negative) subgroups (rs17440077) with monthly lampalizumab treatment versus sham treatment. (**A**) In the *CFI*+ subpopulation, there was a 44% reduction in geographic atrophy area progression with monthly lampalizumab treatment versus sham control at month 18. (**B**) Representative fundus autofluorescence images at baseline and month 18 for the *CFI*+ subpopulation. Relative geographic atrophy area progression is shown for the sham and lampalizumab monthly treated groups. (**C**) In the *CFI*– subpopulation, there was no apparent benefit with monthly lampalizumab treatment versus sham control at month 18. The least-squares mean was estimated from a linear mixed-effect model that included baseline geographic atrophy area as a continuous variable, time point as a categorical variable, treatment, time-by-treatment interaction, and baseline geographic atrophy category (≥10 mm^2 versus <10 mm^2). Vertical bars are 95% CIs of the least-squares mean. In parentheses, *n* corresponds to the number of patients at the 6-, 12-, and 18-month time points, respectively.

every other month, an 18% reduction in geographic atrophy area progression at month 18 was observed relative to the pooled sham subgroup (95% CI, −11 to 47%; $P = 0.2266$; Fig. 5A and table S5). The efficacy observed in the *CFI* risk-allele carrier monthly (44% reduction) and every other month (18% reduction) subgroups appeared to be suggestive of a dose response with lampalizumab (Fig. 5A). Moreover, as observed in the monthly lampalizumab-treated *CFI* risk-negative patients, there was no apparent treatment effect in the *CFI* risk-negative every other month subgroup (Fig. 5B and table S5). We also explored a potential effect of *CFI* risk-allele carrier status on treatment response in patients with better baseline visual acuity (20/50 to 20/100); results from this assessment showed a 54% reduction (95% CI, 21 to 88%; $P = 0.0029$) in geographic atrophy area progression at month 18 with monthly administration of lampalizumab and a 31% reduction (95% CI, −2 to 65%; $P = 0.0676$) in geographic atrophy area progression at month 18 with every other month lampalizumab treatment relative to pooled sham control (table S6). Gender segmentation based on *CFI* risk-allele carrier status was also evaluated in the pooled sham subgroup and showed a more rapid mean change in geographic atrophy area from baseline to month 18 in women versus men (5.02 mm^2 versus 3.18 mm^2, respectively) (table S7); however, the individual lampalizumab treatment benefit for women and men was nevertheless comparable with the combined *CFI* risk-allele carrier monthly subgroup reduction of 44% in geographic atrophy area progression at month 18 relative to the pooled sham control (Fig. 4A).

SNP rs17440077 was selected as a proxy for the published SNP rs4698775 ($r^2 = 0.85$) because it was not on the genotyping platform. Subsequently, we imputed and genotyped SNP rs4698775; efficacy results with SNP rs4698775 were consistent with SNP rs17440077 (fig. S2 and table S8). Rare missense variants of *CFI* have also been reported to be enriched in AMD cases relative to controls (*19*–*21*). In the MAHALO analysis, six patients carried *CFI* missense variants and were equally distributed across the treatment arms; the extremely small sample size prevented a meaningful analysis of the missense variants.

Functional association with the *CFI* risk SNP

SNP rs17440077 is an intronic variant, which is not in linkage disequilibrium with any amino acid coding *CFI* variants. To investigate a potential functional consequence of the risk haplotype defined by SNP rs17440077, we examined whether this variant may be an expression quantitative trait locus (eQTL) affecting messenger RNA (mRNA) expression of endogenous CFI. We analyzed expression data from normal tissues from The Cancer Genome Atlas (TCGA) (*22*). The TCGA database contains both tumor and normal tissue samples;

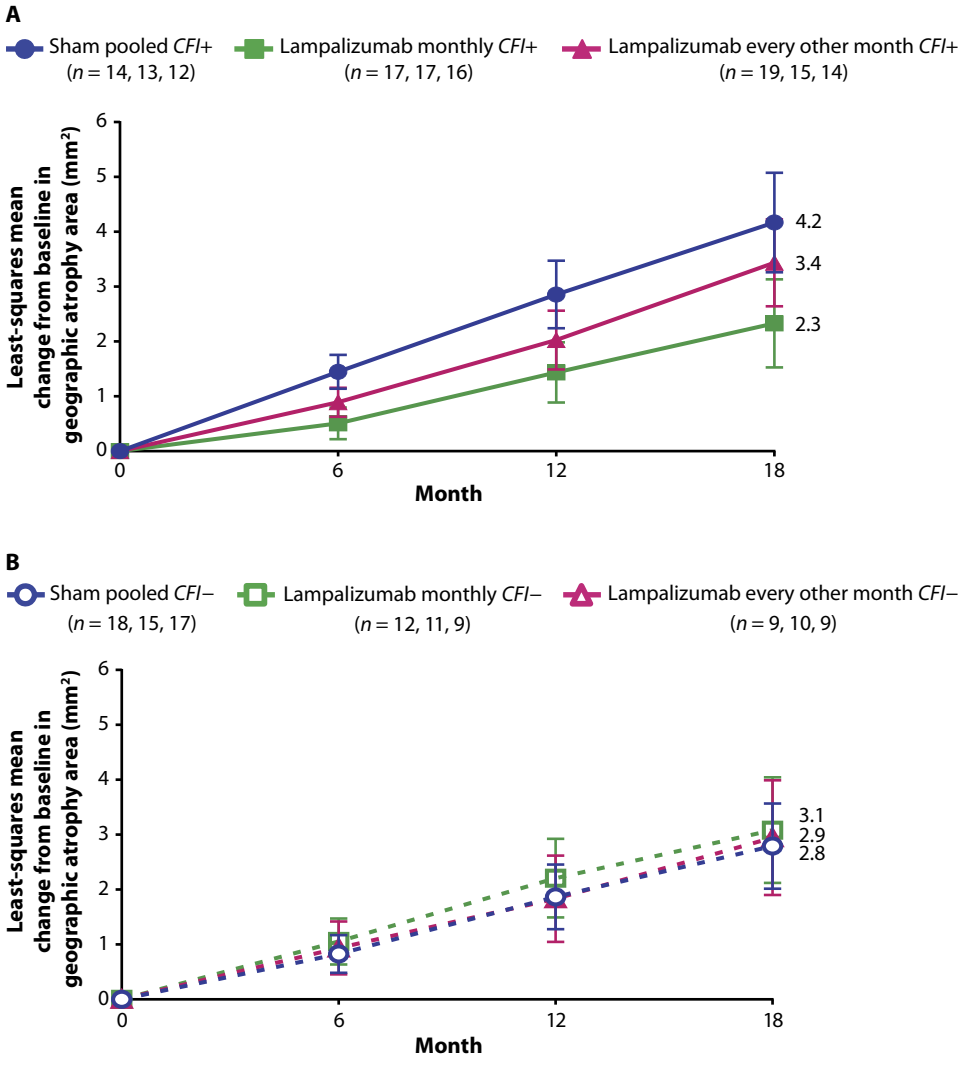

Fig. 5. Geographic atrophy progression in *CFI* risk-allele carriers and risk-negative subpopulations after lampalizumab treatment. Geographic atrophy area by fundus autofluorescence in the *CFI*+ risk-allele carriers (**A**) and *CFI*– risk-negative (**B**) subpopulations (rs17440077) after monthly and every other month lampalizumab treatment versus sham treatment. (A) In the *CFI*+ subpopulation, there was an 18% reduction in geographic atrophy area progression with lampalizumab treatment every other month versus sham control at month 18; moreover, there was a potential dose response between the monthly and every other month lampalizumab treatment subpopulations. (B) Consistent with the *CFI*– monthly lampalizumab subgroup, there was no apparent treatment benefit with every other month lampalizumab treatment versus sham control at month 18. The least-squares mean was estimated from a linear mixed-effect model that included baseline geographic atrophy area as a continuous variable, time point as a categorical variable, treatment, time-by-treatment interaction, and baseline geographic atrophy category (≥10 mm^2 versus <10 mm^2). Vertical bars are 95% CIs of the least-squares mean. In parentheses, *n* corresponds to the number of patients at the 6-, 12-, and 18-month time points, respectively.

however, we only used data from normal tissues to avoid potential tumor effects. The highest expression of *CFI* was in the liver. This is consistent with liver being the site of synthesis for CFI, and this finding was also observed in the BioGPS centralized gene portal (*23*). In 34 TCGA normal liver samples, there was a statistically significant association (P = 0.02) between the SNP rs17440077 genotype and *CFI* expression, with the AA genotype (homozygous risk negative) associated with increased mRNA compared to AG (heterozygous risk carrier) and GG (homozygous risk carrier) genotypes (Fig. 6). This direction of effect is consistent with risk-allele carriers having decreased CFI activity, leading to complement-driven geographic atrophy area progression. As with the geographic atrophy area efficacy analysis, SNP rs4698775 eQTL results (P = 0.02) were consistent with SNP rs17440077. Additionally, we assessed the online Genotype-Tissue Expression (GTEx) expression database portal (*24*); in 97 liver tissue samples, the direction of the effect was aligned with the TCGA-based analysis (P = 0.10).

To further investigate a possible functional effect of the *CFI* SNP, we measured CFI in patient serum from the MAHALO study. In patients with the common *CFI* variant, we did not observe a statistically significant difference in serum CFI concentrations between *CFI* risk-allele carriers and *CFI* risk-negative carriers for rs17440077 (fig. S3) or rs4698775 (fig. S4). However, as with a previous report showing less CFI in the serum of carriers of *CFI* rare amino acid–changing variants (*21*), we found that a subgroup of *CFI* rare variant carriers in the MAHALO study had decreased CFI in serum (figs. S3 and S4). Our eQTL analysis and rare variant serum data suggested that both common and rare risk variants may result in decreased CFI and that odds ratios for these variants should be considered in interpreting these results. The odds ratio for the common variant in the AMD Gene Consortium study is 1.14 (*8*), whereas the odds ratio for the G119R rare variant is 22.20 (*20*). On the basis of these differences, we may anticipate that any observable expression difference would be much more profound in a rare variant carrier, and a small expression difference for the common variant may not be detectable in a serum assay with the relatively small MAHALO sample size. Our results appear to suggest that the transcript-based eQTL approach may be a more powerful method to investigate expression differences for a *CFI* common variant carrier in the MAHALO study. Moreover, steady-state serum concentration of CFI is not only a reflection of transcriptional activity in the liver but also a reflection of protein translation, protein turnover, and biodistribution; these variables may make it challenging to detect small CFI protein differences in serum. For serum analyses, much larger sample sets may be required to detect a significant difference in serum CFI on the basis of the common *CFI* risk allele.

Ocular and systemic safety outcomes

The MAHALO study demonstrated an acceptable safety profile during the 18-month treatment period (Table 2). There were numerically more cases of systemic (nonocular) serious adverse events (SAEs) in the pooled sham group (Table 2). The most common study

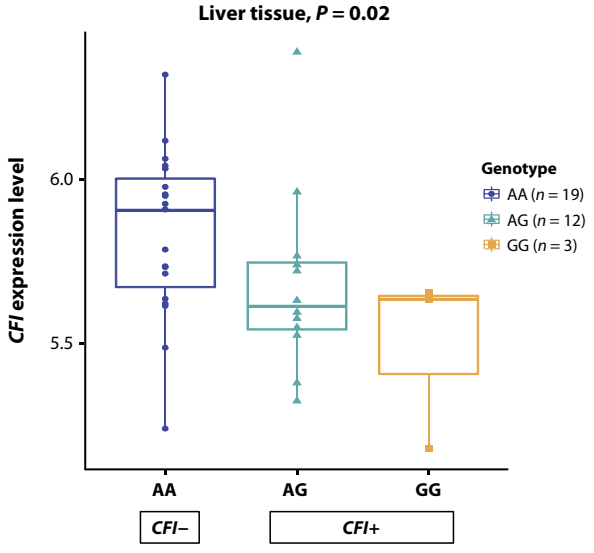

Fig. 6. *CFI* mRNA expression in normal liver tissue differs by rs17440077 genotype. Expression of *CFI* mRNA in tissue from TCGA database (*22*) was analyzed and found to differ according to the rs17440077 genotype. The highest expression of *CFI* mRNA was in the liver, the site of CFI synthesis.

eye ocular adverse events were considered to be associated with the injection procedure (Table 2) and were similar to other agents administered intravitreally. There were no intraocular infections (endophthalmitis), and rates of intraocular inflammation and intraocular pressure elevation were consistent with the anti-VEGF Fab ranibizumab rates in neovascular AMD (*25*). At baseline, the mean study eye intraocular pressure was similar across the sham and lampalizumab monthly and every other month treatment groups. Mean changes from baseline in predose intraocular pressure at each month were negligible for each of the treatment groups in the study eye; most patients had a change of <5 mmHg postdose compared with predose intraocular pressure in the study eye at each treatment visit. There were no unanticipated or unmanageable SAEs reported, and there were no deaths or ocular SAEs suspected to be caused by the study drug. There were no ocular SAEs in the study eye that led to treatment discontinuation. Summaries of ocular adverse events in fellow (nonstudy) eyes, systemic adverse events, and adverse events suspected to be caused by study drug are presented in tables S9 to S11, respectively. As shown in table S11, adverse events suspected to be caused by the study drug based on investigator opinion were minimal; moreover, the vast majority of adverse events suspected to be caused by the study drug were reported as single events with no clear or consistent safety signal. Laboratory test results from serum chemistry, hematology, complement assays, and urinalysis did not identify any patterns of lampalizumab-related effects. The immunogenicity rates for lampalizumab were consistent with the anti-VEGF Fab ranibizumab in neovascular AMD studies (*25*), and there was no apparent anti-therapeutic antibody effect on efficacy, safety, or pharmacokinetics.

Serum, aqueous, and pharmacokinetic analyses

Lampalizumab concentrations in serum samples were quantified to characterize systemic pharmacokinetics. At prespecified time points in lampalizumab-treated patients, observed and model-predicted serum lampalizumab concentrations using a population pharmacokinetics and pharmacodynamics model were well below the minimum concentration required to show transient systemic inhibition of the alternative complement pathway in preclinical studies (table S12) (*26*, *27*). Serum lampalizumab concentrations appeared to reach steady state after the first dose in both the monthly and every other month groups. On the basis of the geometric means of the trough concentration (C_{min})–based accumulation ratios, the monthly and every other month groups did not demonstrate systemic accumulation of lampalizumab between the first dose and subsequent doses as evidenced by accumulation ratios of about 1 (table S13). The noncompartmental and model-based population pharmacokinetic analysis for the MAHALO study showed that the ocular half-life of lampalizumab after intravitreal administration was 6 days, which agrees with the previous results (*13*). In the MAHALO study, we measured CFD and lampalizumab in the aqueous humor and used modeling to predict concentrations of study drug and ocular target suppression in the vitreous humor; this analysis showed that free target (CFD) was substantially suppressed up to day 60 after administration of lampalizumab (*27*). MAHALO population pharmacokinetic analysis showed that once lampalizumab entered the systemic circulation, it was cleared relatively quickly with a serum half-life of about 9 hours (*27*). Furthermore, the pharmacokinetic analysis showed that there were no apparent differences in ocular or serum exposures between *CFI* risk–allele positive and risk-negative subgroups (table S12); these results indicate that pharmacokinetic-related factors did not contribute to the efficacy observed in patients with the *CFI* common risk allele.

DISCUSSION

Geographic atrophy continues to represent a significant unmet medical need because there are no approved or effective treatments for this vision-impairing advanced form of AMD. Various aspects of geographic atrophy have been investigated in mouse models (*6*); however, as a result of inadequate animal models that cannot replicate the complexity and anatomic features of the human disease, discovery and validation of new therapeutic targets for geographic atrophy have focused on human AMD genetic studies. Aberrant activation of the alternative complement pathway has been implicated in the pathogenesis of AMD. Moreover, common variant genetic analyses have demonstrated a strong correlation between the risk of developing AMD and genes regulating the alternative complement pathway, including the critical negative regulators CFH and CFI, as well as CFB and C3. CFD is a pivotal, rate-limiting enzyme that acts early in the alternative complement pathway. The MAHALO study targeted CFD with lampalizumab in patients with geographic atrophy secondary to AMD.

The MAHALO efficacy results represent a potential treatment benefit in reducing geographic atrophy area progression with a complement inhibitor. Moreover, lampalizumab efficacy was increased in a subpopulation of patients: the 20% reduction in geographic atrophy area observed in the monthly lampalizumab all-comer analysis was driven by the 44% reduction in geographic atrophy area in the *CFI* risk-allele carrier subgroup. The MAHALO study results also show that modulating the complement system can alter the course of geographic atrophy, a hypothesis supported by human genetics where common and rare variants in genes of the alternative complement pathway increase risk of AMD. Finally, we report eQTL data as a potential functional association with the *CFI* common risk SNP, where the presence of the risk allele is associated with decreased expression of *CFI* mRNA. As compared with the all-comer MAHALO population, an exploratory subanalysis by *CFI* genotype increased the observed lampalizumab

Table 2. Adverse events in the MAHALO phase 2 clinical trial. All data are *n* (%). AE, adverse event; MedDRA, Medical Dictionary for Regulatory Activities.

Overall profile			
Adverse event	**Sham pooled (*n* = 42)**	**Lampalizumab monthly (*n* = 43)**	**Lampalizumab EOM (*n* = 44)**
Patients with at least one event, *n* (%)			
Ocular SAEs in the study eye	1 (2.4)	0	3 (6.8)
Ocular SAEs in the fellow eye	1 (2.4)	0	2 (4.5)
Systemic (nonocular) SAEs	15 (35.7)	11 (25.6)	10 (22.7)
Ocular AE in the study eye suspected to be caused by study drug	0	4 (9.3)	3 (6.8)
Nonocular AE suspected to be caused by study drug	0	1 (2.3)	1 (2.3)
Ocular adverse events in the study eye (occurring in ≥3 patients in any group; all treated patients)			
MedDRA-preferred term	**Sham pooled (*n* = 42)**	**Lampalizumab monthly (*n* = 43)**	**Lampalizumab EOM (*n* = 44)**
Any ocular AEs in the study eye, *n* (%)	24 (57.1)	36 (83.7)	30 (68.2)
Ocular AEs in the study eye occurring in ≥3 patients in any group, *n* (%)			
AMD	0	2 (4.7)	3 (6.8)
Blepharitis	2 (4.8)	1 (2.3)	6 (13.6)
Cataract	3 (7.1)	2 (4.7)	3 (6.8)
Conjunctival hemorrhage	9 (21.4)	21 (48.8)	15 (34.1)
Conjunctival edema	0	1 (2.3)	3 (6.8)
Dry eye	0	2 (4.7)	3 (6.8)
Eye irritation	1 (2.4)	4 (9.3)	4 (9.1)
Eye pain	4 (9.5)	10 (23.3)	6 (13.6)
Eye pruritus	3 (7.1)	1 (2.3)	3 (6.8)
Foreign body sensation in eyes	1 (2.4)	4 (9.3)	2 (4.5)
Intraocular pressure increased	0	6 (14.0)	7 (15.9)
Lacrimation increased	1 (2.4)	3 (7.0)	4 (9.1)
Ocular hyperemia	2 (4.8)	3 (7.0)	5 (11.4)
Punctate keratitis	1 (2.4)	4 (9.3)	2 (4.5)
Retinal hemorrhage	3 (7.1)	1 (2.3)	3 (6.8)
Vision blurred	1 (2.4)	2 (4.7)	3 (6.8)
Vitreous detachment	3 (7.1)	2 (4.7)	4 (9.1)
Vitreous floaters	1 (2.4)	3 (7.0)	2 (4.5)

treatment effect more than twofold (20% versus 44%) in the monthly group and enabled detection of a treatment effect in the lampalizumab every other month group. Moreover, the magnitude of the lampalizumab treatment benefit in monthly and every other month *CFI* risk-allele carriers was suggestive of a dose response that was not apparent in the all-comer population. Furthermore, although SNP rs17440077 is located within an intron of the gene *CCDC109B*, given the strong complement component associated with AMD risk, *CFI* appears to represent the most plausible causal gene at this locus. Presumably, because of a comparatively lower odds ratio of 1.14 for the strongest associated common SNP at the *CFI* locus in AMD risk, *CFI* has not been considered a major contributor to AMD pathogenesis as compared with the *CFH* and *ARMS2/HTRA1* loci (*8*). However, a recent next-generation sequencing study has shown that rare *CFI* missense mutations are enriched about fourfold in AMD cases compared with controls (*19*). Moreover, another study has shown that this type of variation has a

large impact on AMD risk ($P = 3.9 \times 10^{-6}$; odds ratio, 22.20) (*20*). Additionally, a recent study has examined the relationship between serum CFI and the presence of rare *CFI* missense variants in advanced AMD cases (*21*). This report found that 42% of advanced AMD cases with a rare *CFI* missense variant had lower CFI as compared to 8% of advanced AMD cases without a rare variant. This study also assessed a previously reported common SNP rs10033900 at the *CFI* locus and found no differences in CFI serum concentrations comparing risk-positive and risk-negative homozygotes. Another recent study assessed the effect of SNP rs2285714 at the *CFI* locus on geographic atrophy progression and found no apparent association (*28*). Notably, SNPs rs10033900 and rs2285714 are in relatively strong linkage disequilibrium with each other ($r^2 = 0.78$; table S14) but not with SNPs rs17440077 and rs4698775 ($r^2 < 0.35$; table S14) that were used in the MAHALO analysis. Consistent with the findings in these reports, we did not identify a potential *CFI* marker association or observe differential *CFI* gene expression in eQTL analysis with either SNP rs10033900 or rs2285714. Consequently, whereas the causal variant at the *CFI* locus remains to be determined, SNP rs17440077 (or SNP rs4698775) as tested in the MAHALO study analysis would seem to represent a more plausible candidate or proxy as compared with either SNP rs10033900 or SNP rs2285714 given the observed treatment response in risk-allele carrier MAHALO patients and the apparent differential *CFI* gene expression in the eQTL analysis.

Our data from the MAHALO phase 2 study provide a proof of concept for targeting CFD in patients with geographic atrophy secondary to AMD. As noted, the results of this study involved a relatively limited number of geographic atrophy patients; consequently, conclusions on long-term safety and efficacy of lampalizumab will require more extensive investigation in ongoing phase 3 clinical trials.

A limitation of our study is the relatively small sample size inherent in phase 2 investigations. Our results do not exclude the possibility that *CFI* risk-negative patients may also show benefit from inhibition of complement activity but require increased dosing for evidence of efficacy. Furthermore, although genetic analyses for disease characteristics and treatment response were prespecified, the precise SNPs for the analysis were not predefined. Our observations of the potential predictive effect in geographic atrophy associated with the common *CFI* SNP rs17440077 (or SNP rs4698775) were based on the MAHALO inclusion and exclusion criteria and study population; for meaningful evaluations, comparative analyses in other geographic atrophy study populations should be performed with a randomized design and the MAHALO inclusion and exclusion criteria (for example, baseline geographic atrophy lesion characteristics in the absence of choroidal neovascularization, banded or diffuse fundus autofluorescence patterns, and fellow eye geographic atrophy disease burden). Finally, the MAHALO study was not designed to detect a difference at month 18 in geographic atrophy area progression between the *CFI* risk–allele positive and *CFI* risk-negative sham subgroups; the numerical difference observed at month 18 between these subgroups and a potential prognostic effect will require further assessment in the ongoing phase 3 lampalizumab trials (CHROMA, NCT02247479; SPECTRI, NCT02247531).

The results from the MAHALO phase 2 study provide evidence that targeting CFD in the alternative complement pathway has the potential to be an effective and safe treatment for patients with geographic atrophy secondary to AMD. Our results indicate that modulating the alternative complement pathway can alter the course of geographic atrophy, thus supporting the complement hypothesis in the pathogenesis of AMD.

MATERIALS AND METHODS

Study design

MAHALO was an 18-month multicenter, randomized, single-masked, sham injection–controlled, phase 2 study conducted in the United States (ClinicalTrials.gov identifier, NCT01229215) and Germany (EudraCT number, 2010-019183-36) between May 2011 and April 2013. Institutional review board and ethics committee approval was obtained before study initiation at each of the 32 study sites; all patients provided written informed consent. MAHALO enrolled 129 patients who met the inclusion criteria for the study (Fig. 1). At month 18, patients either continued into the open-label extension study (ClinicalTrials.gov identifier, NCT01602120; EudraCT number, 2012-000578-41) or completed a 3-month safety follow-up period (Fig. 1).

Inclusion criteria

For enrollment, patients had to meet the following major inclusion criteria: age 60 to 89 years; willingness and ability to provide informed consent; for the study eye, best-corrected visual acuity of 20/50 to 20/400 inclusive (Snellen equivalent) using Early Treatment Diabetic Retinopathy Study (ETDRS) charts; for both study and nonstudy eyes, geographic atrophy secondary to AMD in the absence of choroidal neovascularization; for the study eye, a geographic atrophy lesion size of $\geq$2.5 mm^2 and $\leq$17.5 mm^2; geographic atrophy lesion must reside completely within fundus autofluorescence imaging field; banded or diffuse fundus autofluorescence patterns adjacent to the geographic atrophy lesion; and sufficiently clear ocular media.

Exclusion criteria

Major exclusion criteria included the following: geographic atrophy in the study eye that fails to meet lesion size criteria or extends beyond the fundus autofluorescence imaging field, geographic atrophy in either eye due to causes other than AMD, focal or no fundus autofluorescence pattern adjacent to the geographic atrophy lesion, active or history of neovascular AMD, diabetic retinopathy in either eye, active or history of infectious or inflammatory ocular disease in either eye, select ocular and systemic conditions including malignancy, and the use of prohibited concomitant medications.

Randomization, masking, and treatment schedule

Eligible patients were enrolled on day 0 and randomized across four arms using an interactive web response system in a 1:2:1:2 ratio to receive sham monthly injections, intravitreal 10-mg lampalizumab monthly injections, sham every other month injections, or intravitreal 10-mg lampalizumab every other month injections. Because there is risk without potential benefit with a placebo intravitreal injection, sham injections have served as the acceptable control for study drug injections (*29*, *30*). Randomization was stratified by baseline geographic atrophy lesion size, <4 disc areas (<10 mm^2) versus $\geq$4 disc areas ($\geq$10 mm^2). All patients followed a monthly visit schedule regardless of treatment group assignment. Patients, study personnel responsible for performing the best-corrected visual acuity assessment, and the reading center were masked to treatment assignment; the primary efficacy endpoint (geographic atrophy area by fundus autofluorescence) was an objective, quantitative outcome measure that was not influenced by a patient's perception of treatment assignment. Screening eligibility for geographic atrophy lesion characteristics [geographic atrophy secondary to AMD, perilesional autofluorescence patterns (*31*), and geographic atrophy in the absence of choroidal neovascularization] was completed at the GRADE Reading

Center (Bonn, Germany). Geographic atrophy area was measured by fundus autofluorescence, near-infrared imaging, and digitized stereoscopic color fundus photography at screening and at months 6, 12, and 18 by masked graders at the Doheny Image Reading Center (Los Angeles, CA).

Dose selection

The dose for the MAHALO study was selected on the basis of the previous phase 1a study, which demonstrated that a single 10-mg dose of lampalizumab in a 100-μl volume administered by intravitreal injection was safe and well tolerated in study eyes and systemically in patients with geographic atrophy secondary to AMD (*13*). These initial results supported initiation of multidosing with 10 mg of lampalizumab in the MAHALO study. For the every other month lampalizumab arm, justification was based on the predicted vitreous level of lampalizumab at 60 days exceeding the IC_{50} (half-maximal inhibitory concentration) of alternative complement pathway inhibition on a serum hemolytic cell–based assay (*26*). Before initiating the MAHALO phase 2 study, preliminary multidose safety and tolerability of the 10-mg dose were assessed in the open-label phase 1b safety run-in component of the MAHALO study; no dose-limiting toxicities or safety concerns were observed in the safety run-in cohort, permitting subsequent enrollment of the randomized phase 2 study.

Outcome measures

The primary efficacy outcome measure was the mean change in geographic atrophy area from baseline to month 18 assessed by fundus autofluorescence. Secondary outcome measures were mean change in geographic atrophy area from baseline to month 18 assessed by color fundus photography, and mean change in best-corrected visual acuity from baseline to month 18 using the ETDRS chart at a distance of 4 m. Safety outcome measures included the incidence and severity of ocular and systemic adverse events, changes and abnormalities in clinical laboratory parameters, and the incidence of positive serum antibodies to lampalizumab. The pharmacokinetic profile of lampalizumab was also analyzed. As an exploratory outcome measure, genotyping was performed to assess potential relationships between AMD-associated genetic polymorphisms, geographic atrophy disease characteristics, and treatment response to lampalizumab (tables S3 and S4).

Genetic analysis

A single whole-blood sample was collected for genetic marker analysis during the study from patients residing in the United States. Samples were not collected from study centers with policies in place prohibiting collection for genetic marker analysis. Patient samples were genotyped using the Illumina 2.5M Omni SNP array (Illumina Inc.). From this set of genotypes, four SNPs were selected to test for lampalizumab response from confirmed AMD genetic risk loci containing genes in the complement pathway: one SNP each for *CFH*, *CFI*, and *C3*, and one tagging both *C2* and *CFB* (referred to as *C2/CFB*). These SNPs were selected according to a recent meta-analysis by the AMD Gene Consortium consisting of >17,000 AMD cases compared with >60,000 unaffected controls (*8*). Published index SNPs at *C3* (rs2230199) and *C2/CFB* (rs429608) were present in our data set after implementation of quality control measures. However, the published SNPs for *CFH* (rs10737680) and *CFI* (rs4698775) (*8*) were not present. We selected corresponding surrogate SNPs present in our data set after quality control through assessment of linkage disequilibrium patterns in the CEU HapMap population (Utah residents with ancestry from northern and western Europe) (*32*) for *CFH* (rs1329428; $r^2 = 1.0$, $D' = 1.0$ with published SNP rs10737680) and *CFI* (rs17440077; $r^2 = 0.85$, $D' = 0.94$ with published SNP rs4698775). Risk-allele status was determined by comparing the allele frequency of the tagSNPs with the frequency of the effect allele in the AMD Gene study (*8*).

eQTL analysis

TCGA RNA sequencing (RNA-seq) data were obtained from the Cancer Genomics Hub at the University of California, Santa Cruz (Santa Cruz, CA). Here, we used 34 samples of normal liver tissue. RNA-seq data for these were analyzed using HTSeqGenie (*33*) as follows: first, reads with low nucleotide qualities were removed (70% of bases with quality <23). The reads that passed were then aligned to the reference genome GRCh37 using gsnap (*34*). Alignments of the reads that were reported by gsnap as "uniquely mapping" were used for subsequent analysis. *CFI* gene expression level for each sample was then quantified in terms of reads per kilobase of exon model per million mapped reads (RPKM) = number of reads aligning to *CFI* gene/(total number of uniquely mapped reads for the samples × *CFI* gene length). Genotype data for these samples were obtained from dbGap and included genotypes for the Affymetrix 6.0 (1 million) SNP array. Association analysis was then carried out, which included performing linear regression of log(*CFI* RPKM) on the rs17440077 genotype coded additively (that is, zero, one, and two copies of "G" allele).

GTEx data used in our analysis were obtained from the online GTEx Portal (*24*) (www.gtexportal.org/home/testyourown). The search was conducted on 20 April 2016; the command entered was rs17440077, CFI, Liver.

CFI immunoassay

Nunc MaxiSorp plates were coated with anti-human CFI antibody (Complement Technology Inc., catalog #A238) overnight at 4°C. Plates were then washed with wash buffer [phosphate-buffered saline (PBS) + 0.01% Tween-20] and blocked with blocking buffer [3% bovine serum albumin (BSA) in wash buffer] for 1 hour at room temperature. Plates were again washed with wash buffer, and 100 μl of a CFI standard (purified CFI; CompTech, catalog #A138) or a human serum sample diluted 1:5000 in sample diluent (1% BSA in PBS + 0.05% Tween-20) was added and incubated for 2 hours at room temperature. Plates were washed again with wash buffer, and 100 μl of detection antibody (murine anti-human CFI; Quidel, catalog #A237) was added and incubated for 1 hour at room temperature. Plates were washed with wash buffer, and 100 μl of goat anti-mouse horseradish peroxidase (HRP) antibody (BD Pharmingen, catalog #554002) was added and incubated for 1 hour at room temperature. Plates were then washed with wash buffer, and 100 μl of tetramethylbenzidine (TMB) substrate (Thermo Fisher, catalog #34021) was added and incubated for 20 min at room temperature. Fifty microliters of 2N H_2SO_4 was added to wells to stop the reaction. Absorbance was measured at 450 nm with wavelength correction at 570 nm on a VersaMax plate reader.

Serum lampalizumab analysis

The total concentrations of lampalizumab in human serum were measured by enzyme-linked immunosorbent assay (ELISA). A mouse mAb to lampalizumab (clone 7470, Genentech Inc.) that allows for detection of free lampalizumab and lampalizumab bound to CFD was diluted to 1 μg/ml in coating buffer (0.05 M sodium carbonate buffer, pH 9.6), added to microtiter plates (Nunc MaxiSorp, Thermo Scientific), and incubated overnight at 4°C. The standard curve was

prepared in 10% normal human serum (BioreclamationIVT) containing mouse immunoglobulin G (IgG) (50 μg/ml; Equitech-Bio Inc.). Assay controls and samples were diluted at a minimum of 1:10 in assay buffer containing mouse IgG (50 μg/ml). Standards, controls, and samples were added to the plates and incubated overnight at room temperature. Human CFD (100 ng/ml; Complement Technology Inc.), biotin-labeled mouse mAb to CFD (clone 4676, Genentech Inc.), high-sensitivity streptavidin-HRP (Thermo Scientific), and tetrabutylammonium borohydride substrate (Kirkegaard & Perry Laboratories Inc.) were sequentially added, and the reaction was stopped with 1 M phosphoric acid. Plates were read using a microplate reader (SpectraMax 190; Molecular Devices LLC), and lampalizumab concentrations were calculated from a four-parameter fit of the standard curve on each plate (SoftMax Pro; Molecular Devices LLC). The minimum quantifiable lampalizumab concentration in human serum was 350 pg/ml.

Aqueous lampalizumab analysis

The total concentrations of lampalizumab in human aqueous humor were measured by ELISA. A mouse mAb to lampalizumab (clone 7470, Genentech Inc.) that allows for detection of free lampalizumab and lampalizumab bound to CFD was diluted to 2 μg/ml in coating buffer (0.05 M sodium carbonate buffer, pH 9.6), added to microtiter plates (Nunc MaxiSorp, Thermo Scientific), and incubated overnight at 4°C. The standard curve was prepared in assay buffer containing mouse IgG (50 μg/ml; Equitech-Bio Inc.). Assay controls and samples were diluted at a minimum of 1:100 in assay buffer containing mouse IgG. Standards, controls, and samples were added to the plates and incubated for 2 hours at room temperature. Human CFD (50 ng/ml; Complement Technology Inc.), HRP-labeled mouse mAb to CFD (clone 4676, Genentech Inc.), and TMB substrate (Kirkegaard & Perry Laboratories Inc.) were sequentially added, and the reaction was stopped with 1 M phosphoric acid. Plates were read using a microplate reader (SpectraMax 190; Molecular Devices LLC), and lampalizumab concentrations were calculated from a four-parameter fit of the standard curve on each plate (SoftMax Pro; Molecular Devices). The minimum quantifiable lampalizumab concentration in human serum was 30 ng/ml.

Pharmacokinetic analysis

Pharmacokinetic parameters were analyzed using noncompartmental analysis and model-based population pharmacokinetic/pharmacodynamic (PK/PD) analysis. An extensive model-based population PK/PD analysis has been reported elsewhere (*27*) and was used to predict serum and aqueous concentrations over the entire time course to enable peak concentration (C_{max}) and area under the curve (AUC) calculation. Noncompartmental pharmacokinetic analysis was used to evaluate drug concentration data and determine AUC over the 18-month course of lampalizumab treatment ($AUC_{0–18m}$), C_{max}, C_{min}, and half-life. Serum drug concentrations of lampalizumab that measured lower than the lower limit of quantification (LLOQ) were assigned a value of 50% of the LLOQ.

Statistical analysis

All efficacy analyses were conducted in the mITT population, defined as all randomized patients who received at least one dose of treatment and had at least one post-baseline fundus autofluorescence measurement. Prespecified analyses of the primary endpoint were performed using a stratified ANOVA model with baseline geographic atrophy lesion size as the stratification variable; missing data were imputed using the LOCF method. Sensitivity analyses were performed using a linear mixed-effect model with a random effect for each patient based on observed data. The linear mixed-effect model included baseline geographic atrophy area (as the continuous variable), time point (as the categorical variable), treatment, time-by-treatment interaction, and baseline geographic atrophy category ($\geq$10 mm^2 versus <10 mm^2). This approach made use of data from patients who had post-baseline measurements but discontinued the study before month 18 and provided more precise estimation of treatment effect. Sensitivity analyses using a linear mixed-effect model with intercept and time as random effects were also performed (tables S15 and S16). A major objective of this study was to investigate evidence of activity of lampalizumab in geographic atrophy patients. Given the relatively small sample size of proof-of-concept studies including the MAHALO study, there was no formal statistical comparison of reduction in geographic atrophy area progression between the monthly and every other month lampalizumab treatment groups; moreover, no multiplicity adjustment was made for efficacy analyses. All analyses were performed using SAS (version 9.2; SAS Institute Inc.). All efficacy endpoints were evaluated independently for each lampalizumab treatment group compared with the prespecified pooled sham analysis group. The MAHALO efficacy data were also analyzed by the square root transformation method (*35*). The adjusted mean change from baseline to month 18 by the square root transformation method was 0.5, 0.4, and 0.5 mm^2 in the pooled sham, lampalizumab monthly, and every other month groups, respectively. In the CFI risk-allele carrier subgroup, the adjusted mean change from baseline to month 18 was 0.7, 0.4, and 0.6 mm^2 in corresponding treatment groups. The reduction in geographic atrophy area growth was about 20% (80% CI, 1 to 29%) in the lampalizumab primary analysis monthly group and 43% (95% CI, 17 to 70%) in the CFI risk-allele carriers treated with monthly lampalizumab. These results with the square root transformation method were consistent with findings from the least-squares mean primary and subgroup efficacy analyses. To assess the impact of missing data, we performed sensitivity analyses with various imputations methods; the treatment difference between lampalizumab and the pooled sham groups (reduction rate) was consistent across the sensitivity analyses (table S17). Safety data were summarized for all randomized patients who received at least one injection; patients were assessed according to actual treatment received by use of observed data without imputation. The sample size calculation for the MAHALO study was designed to provide power (80%) to detect a treatment effect of 0.94 mm^2/year on geographic atrophy area progression at a two-sided significance level of 0.2. An SD of 1.7 mm^2/year based on available literature (*31*) and a projected 25% dropout rate were assumed in calculating the sample size of 40 patients in lampalizumab monthly and lampalizumab every other month treatment groups, and 40 patients in the pooled sham control with 20 patients each in sham monthly and sham every other month groups.

SUPPLEMENTARY MATERIALS

www.sciencetranslationalmedicine.org/cgi/content/full/9/395/eaaf1443/DC1

Fig. S1. Kaplan-Meier plot of time to study discontinuation by treatment group.

Fig. S2. Geographic atrophy progression with monthly and every other month lampalizumab treatment.

Fig. S3. Average CFI serum concentrations by rs17440077 genotype.

Fig. S4. Average CFI serum concentrations by rs4698775 genotype.

Table S1. Mean change in geographic atrophy area from baseline to month 18 by fundus autofluorescence and color fundus photography based on the mITT population (LOCF method).

Table S2. Least-squares mean change in best-corrected visual acuity from baseline based on the mITT population using LOCF data.

Table S3. SNP genotype counts and allele frequencies for patients assayed in the MAHALO study.
Table S4. Least-squares mean change in geographic atrophy area from baseline to month 18 by risk-allele status.
Table S5. Least-squares mean change in geographic atrophy area (mm^2) by fundus autofluorescence from baseline by *CFI* status (rs17440077) based on the mITT population (observed data).
Table S6. Geographic atrophy progression by fundus autofluorescence in *CFI*+ subgroups (rs17440077) with monthly and every other month lampalizumab treatment versus sham control and baseline best-corrected visual acuity of 20/50 to 20/100 (Snellen equivalent).
Table S7. Least-squares mean change in geographic atrophy area (mm^2) from baseline to month 18 by gender: *CFI* risk-allele carriers in mITT patients.
Table S8. Least-squares mean change in geographic atrophy area (mm^2) by fundus autofluorescence from baseline by *CFI* status (rs4698775) based on the mITT population (observed data).
Table S9. Ocular adverse events in the fellow eye during the 18-month treatment period occurring among ≥3 patients in any treatment group (safety-evaluable patients).
Table S10. Systemic (nonocular) adverse events during the 18-month treatment period occurring among ≥3 patients in any treatment group (safety-evaluable patients).
Table S11. Adverse events suspected to be caused by study drug during the 18-month treatment period (safety-evaluable patients).
Table S12. Serum and aqueous exposures in lampalizumab-treated patients.
Table S13. Summary of estimated accumulation ratios in lampalizumab-treated patients.
Table S14. *CFI* SNPs and relationships.
Table S15. Predicted mean change in geographic atrophy area from baseline: mITT patients.
Table S16. Predicted mean change in geographic atrophy area from baseline by *CFI* status: mITT patients.
Table S17. Least-squares mean change in geographic atrophy area from baseline to month 18 (study eye): mITT patients.
Source data

REFERENCES AND NOTES

1. L. S. Lim, P. Mitchell, J. M. Seddon, F. G. Holz, T. Y. Wong, Age-related macular degeneration. *Lancet* **379**, 1728–1738 (2012).
2. W. L. Wong, X. Su, X. Li, C. M. Cheung, R. Klein, C.-Y. Cheng, T. Y. Wong, Global prevalence of age-related macular degeneration and disease burden projection for 2020 and 2040: A systematic review and meta-analysis. *Lancet Glob. Health* **2**, e106–e116 (2014).
3. J. S. Sunness, G. S. Rubin, C. A. Applegate, N. M. Bressler, M. J. Marsh, B. S. Hawkins, D. Haselwood, Visual function abnormalities and prognosis in eyes with age-related geographic atrophy of the macula and good visual acuity. *Ophthalmology* **104**, 1677–1691 (1997).
4. F. G. Holz, E. C. Strauss, S. Schmitz-Valckenberg, M. van Lookeren Campagne, Geographic atrophy: Clinical features and potential therapeutic approaches. *Ophthalmology* **121**, 1079–1091 (2014).
5. F. G. Holz, S. Schmitz-Valckenberg, M. Fleckenstein, Recent developments in the treatment of age-related macular degeneration. *J. Clin. Invest.* **124**, 1430–1438 (2014).
6. M. van Lookeren Campagne, J. LeCouter, B. L. Yaspan, W. Ye, Mechanisms of age-related macular degeneration and therapeutic opportunities. *J. Pathol.* **232**, 151–164 (2014).
7. M. B. Gorin, Genetic insights into age-related macular degeneration: Controversies addressing risk, causality, and therapeutics. *Mol. Aspects Med.* **33**, 467–486 (2012).
8. L. G. Fritsche, W. Chen, M. Schu, B. L. Yaspan, Y. Yu, G. Thorleifsson, D. J. Zack, S. Arakawa, V. Cipriani, S. Ripke, R. P. Igo Jr., G. H. S. Buitendijk, X. Sim, D. E. Weeks, R. H. Guymer, J. E. Merriam, P. J. Francis, G. Hannum, A. Agarwal, A. M. Armbrecht, I. Audo, T. Aung, G. R. Barile, M. Benchaboune, A. C. Bird, P. N. Bishop, K. E. Branham, M. Brooks, A. J. Brucker, W. H. Cade, M. S. Cain, P. A. Campochiaro, C.-C. Chan, C.-Y. Cheng, E. Y. Chew, K. A. Chin, I. Chowers, D. G. Clayton, R. Cojocaru, Y. P. Conley, B. K. Cornes, M. J. Daly, B. Dhillon, A. O. Edwards, E. Evangelou, J. Fagerness, H. A. Ferreyra, J. S. Friedman, A. Geirsdottir, R. J. George, C. Gieger, N. Gupta, S. A. Hagstrom, S. P. Harding, C. Haritoglou, J. R. Heckenlively, F. G. Holz, G. Hughes, J. P. A. Ioannidis, T. Ishibashi, P. Joseph, G. Jun, Y. Kamatani, N. Katsanis, C. N. Kielhauer, J. C Khan, I. K. Kim, Y. Kiyohara, B. E. K. Klein, R. Klein, J. L. Kovach, I. Kozak, C. J. Lee, K. E. Lee, P. Lichtner, A. J. Lotery, T. Meitinger, P. Mitchell, S. Mohand-Saïd, A. T. Moore, D. J. Morgan, M. A. Morrison, C. E. Myers, A. C. Naj, Y. Nakamura, Y. Okada, A. Orlin, M. C. Ortube, M. I. Othman, C. Pappas, K. H. Park, G. J. T. Pauer, N. S. Peachey, O. Poch, R. R. Priya, R. Reynolds, A. J. Richardson, R. Ripp, G. Rudolph, E. Ryu, J.-A. Sahel, D. A. Schaumberg, H. P. N. Scholl, S. G. Schwartz, W. K. Scott, H. Shahid, H. Sigurdsson, G. Silvestri, T. A. Sivakumaran, R. T. Smith, L. Sobrin, E. H. Souied, D. E. Stambolian, H. Stefansson, G. M. Sturgill-Short, A. Takahashi, N. Tosakulwong, B. J. Truitt, E. E. Tsironi, A. G. Uitterlinden, C. M. van Duijn, L. Vijaya, J. R. Vingerling, E. N. Vithana, A. R. Webster, H. E. Wichmann, T. W. Winkler, T. Y. Wong, A. F. Wright, D. Zelenika, M. Zhang, L. Zhao, K. Zhang, M. L. Klein, G. S. Hageman, G. M. Lathrop, K. Stefansson, R. Allikmets, P. N. Baird, M. B. Gorin, J. J. Wang, C. C. W. Klaver, J. M. Seddon, M. A. Pericak-Vance, S. K. Iyengar, J. R. W. Yates, A. Swaroop, B. H. F. Weber, M. Kubo, M. M. Deangelis, T. Leveillard, U. Thorsteinsdottir, J. L. Haines, L. A. Farrer, I. M. Heid, G. R. Abecasis, Seven new loci associated with age-related macular degeneration. *Nat. Genet.* **45**, 433–439 (2013).
9. D. Ricklin, G. Hajishengallis, K. Yang, J. D. Lambris, Complement: A key system for immune surveillance and homeostasis. *Nat. Immunol.* **11**, 785–797 (2010).
10. K. M. Loyet, L. E. Deforge, K. J. Katschke Jr., L. Diehl, R. R. Graham, L. Pao, L. Sturgeon, S.-C. Lewin-Koh, J. G. Hollyfield, M. van Lookeren Campagne, Activation of the alternative complement pathway in vitreous is controlled by genetics in age-related macular degeneration. *Invest. Ophthalmol. Vis. Sci.* **53**, 6628–6637 (2012).
11. C. M. Stanton, J. R. W. Yates, A. I. den Hollander, J. M. Seddon, A. Swaroop, D. Stambolian, S. Fauser, C. Hoyng, Y. Yu, K. Atsuhiro, K. Branham, M. Othman, W. Chen, E. Kortvely, K. Chalmers, C. Hayward, A. T. Moore, B. Dhillon, M. Ueffing, A. F. Wright, Complement factor D in age-related macular degeneration. *Invest. Ophthalmol. Vis. Sci.* **52**, 8828–8834 (2011).
12. H. P. N. Scholl, P. Charbel Issa, M. Walier, S. Janzer, B. Pollok-Kopp, F. Börncke, L. G. Fritsche, N. V. Chong, R. Fimmers, T. Wienker, F. G. Holz, B. H. F. Weber, M. Oppermann, Systemic complement activation in age-related macular degeneration. *PLOS ONE* **3**, e2593 (2008).
13. D. V. Do, D. J. Pieramici, M. van Lookeren Campagne, T. Beres, M. Friesenhahn, Y. Zhang, E. C. Strauss, A phase IA dose-escalation study of the anti-factor D monoclonal antibody fragment FCFD4514S in patients with geographic atrophy. *Retina* **34**, 313–320 (2014).
14. K. J. Katschke Jr., P. Wu, R. Ganesan, R. F. Kelley, M. A. Mathieu, P. E. Hass, J. Murray, D. Kirchhofer, C. Wiesmann, M. van Lookeren Campagne, Inhibiting alternative pathway complement activation by targeting the factor D exosite. *J. Biol. Chem.* **287**, 12886–12892 (2012).
15. E. C. Schramm, S. J. Clark, M. P. Triebwasser, S. Raychaudhuri, J. M. Seddon, J. P. Atkinson, Genetic variants in the complement system predisposing to age-related macular degeneration: A review. *Mol. Immunol.* **61**, 118–125 (2014).
16. S. McHarg, S. J. Clark, A. J. Day, P. N. Bishop, Age-related macular degeneration and the role of the complement system. *Mol. Immunol.* **67**, 43–50 (2015).
17. L. Rubinstein, J. Crowley, P. Ivy, M. Leblanc, D. Sargent, Randomized phase II designs. *Clin. Cancer Res.* **15**, 1883–1890 (2009).
18. S. A. Cannistra, Phase II trials in journal of clinical oncology. *J. Clin. Oncol.* **27**, 3073–3076 (2009).
19. J. M. Seddon, Y. Yu, E. C. Miller, R. Reynolds, P. L. Tan, S. Gowrisankar, J. I. Goldstein, M. Triebwasser, H. E. Anderson, J. Zerbib, D. Kavanagh, E. Souied, N. Katsanis, M. J. Daly, J. P. Atkinson, S. Raychaudhuri, Rare variants in *CFI*, *C3* and *C9* are associated with high risk of advanced age-related macular degeneration. *Nat. Genet.* **45**, 1366–1370 (2013).
20. J. P. H. van de Ven, S. C. Nilsson, P. L. Tan, G. H. Buitendijk, T. Ristau, F. C. Mohlin, S. B. Nabuurs, F. E. Schoenmaker-Koller, D. Smailhodzic, P. A. Campochiaro, D. J. Zack, M. R. Duvvari, B. Bakker, C. C. Paun, C. J. F. Boon, A. G. Uitterlinden, S. Liakopoulos, B. J. Klevering, S. Fauser, M. R. Daha, N. Katsanis, C. C. W. Klaver, A. M. Blom, C. B. Hoyng, A. I. den Hollander, A functional variant in the *CFI* gene confers a high risk of age-related macular degeneration. *Nat. Genet.* **45**, 813–817 (2013).
21. D. Kavanagh, Y. Yu, E. C. Schramm, M. Triebwasser, E. K. Wagner, S. Raychaudhuri, M. J. Daly, J. P. Atkinson, J. M. Seddon, Rare genetic variants in the *CFI* gene are associated with advanced age-related macular degeneration and commonly result in reduced serum factor I levels. *Hum. Mol. Genet.* **24**, 3861–3870 (2015).
22. The Cancer Genome Atlas Research Network, The Cancer Genome Atlas; http://cancergenome.nih.gov [accessed 16 December 2014].
23. C. Wu, C. Orozco, J. Boyer, M. Leglise, J. Goodale, S. Batalov, C. L. Hodge, J. Haase, J. Janes, J. W. Huss III, A. I. Su, BioGPS: An extensible and customizable portal for querying and organizing gene annotation resources. *Genome Biol.* **10**, R130 (2009).
24. GTEx Consortium, The Genotype-Tissue Expression (GTEx) pilot analysis: Multitissue gene regulation in humans. *Science* **348**, 648–660 (2015).
25. Genentech Inc., Lucentis® (ranibizumab injection); www.gene.com/download/pdf/lucentis_prescribing.pdf [accessed 13 February 2015].
26. K. M. Loyet, J. Good, T. Davancaze, L. Sturgeon, X. Wang, J. Yang, K. N. Le, M. Wong, P. E. Hass, M. van Lookeren Campagne, P. C. Haughney, A. Morimoto, L. A. Damico-Beyer, L. E. DeForge, Complement inhibition in cynomolgus monkeys by anti–factor D antigen-binding fragment for the treatment of an advanced form of dry age-related macular degeneration. *J. Pharmacol. Exp. Ther.* **351**, 527–537 (2014).
27. K. N. Le, L. Gibiansky, M. van Lookeren Campagne, J. Good, T. Davancaze, K. M. Loyet, A. Morimoto, E. C. Strauss, J. Y. Jin, Population pharmacokinetics and pharmacodynamics of lampalizumab administered intravitreally to patients with geographic atrophy. *Clin. Pharmacol. Ther. Pharmacometrics Syst. Pharmacol.* **4**, 595–604 (2015).
28. F. Grassmann, M. Fleckenstein, E. Y. Chew, T. Strunz, S. Schmitz-Valckenberg, A. P. Göbel, M. L. Klein, R. Ratnapriya, A. Swaroop, F. G. Holz, B. H. F. Weber, Clinical and genetic factors associated with progression of geographic atrophy lesions in age-related macular degeneration. *PLOS ONE* **10**, e0126636 (2015).
29. D. M. Brown, P. K. Kaiser, M. Michels, G. Soubrane, J. S. Heier, R. Y. Kim, J. P. Sy, S. Schneider, Ranibizumab versus verteporfin for neovascular age-related macular degeneration. *N. Engl. J. Med.* **355**, 1432–1444 (2006).

30. P. J. Rosenfeld, D. M. Brown, J. S. Heier, D. S. Boyer, P. K. Kaiser, C. Y. Chung, R. Y. Kim; Marina Study Group, Ranibizumab for neovascular age-related macular degeneration. *N. Engl. J. Med.* **355**, 1419–1431 (2006).
31. F. G. Holz, A. Bindewald-Wittich, M. Fleckenstein, J. Dreyhaupt, H. P. N. Scholl, S. Schmitz-Valckenberg, Progression of geographic atrophy and impact of fundus autofluorescence patterns in age-related macular degeneration. *Am. J. Ophthalmol.* **143**, 463–472.e2 (2007).
32. The International HapMap Consortium, A haplotype map of the human genome. *Nature* **437**, 1299–1320 (2005).
33. G. Pau, J. Reeder, HTSeqGenie: A NGS analysis pipeline. R package version 3.18.0; http://bioconductor.org/packages/release/bioc/html/HTSeqGenie.html [accessed 9 July 2015].
34. T. D. Wu, S. Nacu, Fast and SNP-tolerant detection of complex variants and splicing in short reads. *Bioinformatics* **26**, 873–881 (2010).
35. W. J. Feuer, Z. Yehoshua, G. Gregori, F. M. Penha, E. Y. Chew, F. L. Ferris, T. E. Clemons, A. S. Lindblad, P. J. Rosenfeld, Square root transformation of geographic atrophy area measurements to eliminate dependence of growth rates on baseline lesion measurements: A reanalysis of age-related eye disease study report no. 26. *JAMA Ophthalmol.* **131**, 110–111 (2013).

Acknowledgments: We thank J. Good, T. Davancaze, and C. Amaya for contributions to bioanalytical studies and J. Martin for review of the safety data. Support for third-party writing assistance for this manuscript, furnished by M. Kelly, CMPP, of Envision Pharma Group, was provided by Genentech Inc. **Funding:** Genentech Inc. supported and contributed to all aspects of the study, including the study design, data collection and analyses, statistical analyses, data interpretation, and report writing. Support for third-party writing assistance for this article was provided by the sponsor. All authors had access to the data, contributed to the manuscript, and provided approval for publication. The corresponding author had final responsibility for the decision to submit the manuscript for publication.
Author contributions: E.C.S., T.B., Z.L., K.N.L., and R.R.G. contributed to the study design; Z.L., E.C.S., and T.B. contributed to safety and efficacy data acquisition; B.L.Y. and A.D. contributed to genetic data acquisition; K.N.L. contributed to pharmacokinetic data acquisition; T.R.B. contributed to eQTL data acquisition; L.A.H. and A.S. contributed to serum and aqueous data acquisition; D.F.W., F.G.H., and C.D.R. contributed to clinical examination data acquisition; E.C.H. contributed to enrollment and retention data acquisition; and Z.L., E.C.S., C.H., B.L.Y., A.D., R.R.G., K.N.L., M.v.L.C., T.R.B., L.A.H., and A.S. contributed to data analysis. All authors contributed to data interpretation and critically reviewed and approved the manuscript. **Competing interests:** B.L.Y., Z.L., A.D., M.v.L.C., R.R.G., T.B., T.R.B., E.C.H., L.A.H., and E.C.S. are employees of Genentech Inc. and have Roche stock/stock options. K.N.L., A.S., and C.H. were employees of Genentech Inc. at the time of the MAHALO study and during manuscript development; K.N.L. is currently an employee of Agios Pharmaceuticals, and C.H. is currently an employee of Denali Therapeutics. D.F.W. has received advisory board funds from Genentech Inc. and is a cofounder/owner of Vestrum Health (financial contractual relationship with Genentech Inc.). F.G.H. has received research support from Allergan, Bayer, Genentech Inc., Heidelberg Engineering, Novartis, and Roche and consulted for Alcon, Bayer, Genentech Inc., Heidelberg Engineering, Novartis, and Roche. C.D.R. has received research support from Acucela, Allergan, Genentech Inc., GlaxoSmithKline, Ocata, Regeneron, and ThromboGenics and consulted for Acucela, Allergan, Genentech Inc., Regeneron, and ThromboGenics. A patent (#CA2920666 A1) has been granted entitled "Compositions and method for treating complement-associated conditions."

MAHALO Study Investigators: H. Agostini, University Medical Center Freiburg, Freiburg, Germany; A. Antoszyk, Charlotte Eye, Ear, Nose and Throat Associates, Charlotte, NC, USA; K. U. Bartz-Schmidt, University of Tübingen, Tübingen, Germany; B. Berger, Retina Research Center, Austin, TX, USA; D. Boyer, Retina-Vitreous Associates Medical Group, Los Angeles, CA, USA; A. Brucker, Scheie Eye Institute, Philadelphia, PA, USA; B. Busbee, Tennessee Retina, P.C., Nashville, TN, USA; P. Campochiaro, The Wilmer Eye Institute, Johns Hopkins University School of Medicine, Baltimore, MD, USA; T. Connor, Medical College of Wisconsin, Milwaukee, WI, USA; K. Csaky, Texas Retina Associates, Dallas, TX, USA; S. Dithmar, Heidelberg University, Heidelberg, Germany; D. Do, The Wilmer Eye Institute, Johns Hopkins University School of Medicine, Baltimore, MD, USA; R. Dreyer, Retina Northwest, Portland, OR, USA; A. Fu, West Coast Retina, San Francisco, CA, USA; R. Gallemore, Retina Macula Institute, Torrance, CA, USA; S. Gupta, Retina Specialty Institute, Pensacola, FL, USA; L. Halperin, Retina Group of Florida, Fort Lauderdale, FL, USA; J. Heier, Ophthalmic Consultants of Boston, Boston, MA, USA; F. Holz, University of Bonn, Bonn, Germany; H. Hudson, Retina Centers P.C., Tucson, AZ, USA; R. Katz, Florida Eye, Boynton Beach, FL, USA; D. Marcus, Southeast Retina Center, Augusta, GA, USA; M. Michels, Retina Care Specialists, Palm Beach Gardens, FL, USA; D. Miller, Cincinnati Eye Institute, Cincinnati, OH, USA; S. Patel, Retina Research Institute of Texas, Abilene, TX, USA; D. Pauleikhoff, St. Franziskus-Hospital, Münster, Germany; D. Pieramici, California Retina Consultants, Santa Barbara, CA, USA; C. Regillo, Wills Eye Hospital, Philadelphia, PA, USA; L. Singerman, Retina Associates of Cleveland, Cleveland, OH, USA; G. Stoller, Ophthalmic Consultants of Long Island, Lynbrook, NY, USA; M. Tolentino, Center for Retina and Macular Disease, Winter Haven, FL, USA; P. Wiedemann, University of Leipzig, Leipzig, Germany; D. Williams, VitreoRetinal Surgery PA, Minneapolis, MN, USA.

Submitted 22 December 2015
Resubmitted 27 May 2016
Accepted 30 January 2017
Published 21 June 2017
10.1126/scitranslmed.aaf1443

Citation: B. L. Yaspan, D. F. Williams, F. G. Holz, C. D. Regillo, Z. Li, A. Dressen, M. van Lookeren Campagne, K. N. Le, R. R. Graham, T. Beres, T. R. Bhangale, L. A. Honigberg, A. Smith, E. C. Henry, C. Ho, E. C. Strauss; for the MAHALO Study Investigators, Targeting factor D of the alternative complement pathway reduces geographic atrophy progression secondary to age-related macular degeneration. *Sci. Transl. Med.* **9**, eaaf1443 (2017).

Science Translational Medicine

Targeting factor D of the alternative complement pathway reduces geographic atrophy progression secondary to age-related macular degeneration

Brian L. Yaspan, David F. Williams, Frank G. Holz, Carl D. Regillo, Zhengrong Li, Amy Dressen, Menno van Lookeren Campagne, Kha N. Le, Robert R. Graham, Tatiana Beres, Tushar R. Bhangale, Lee A. Honigberg, Ashley Smith, Erin C. Henry, Carole Ho, Erich C. Strauss and for the MAHALO Study Investigators

Sci Transl Med **9**, eaaf1443.
DOI: 10.1126/scitranslmed.aaf1443

Illuminating a new treatment for macular degeneration

Geographic atrophy secondary to age-related macular degeneration is a major cause of vision loss for which there is no treatment. Yaspan *et al.* now report the results of the MAHALO phase 2 randomized, controlled trial that evaluated lampalizumab in patients with geographic atrophy secondary to age-related macular degeneration. Lampalizumab is a specific inhibitor of complement factor D, a pivotal regulator of the alternative complement pathway. The MAHALO study met its primary efficacy endpoint with a 20% reduction in lesion area progression compared to sham control with monthly lampalizumab treatment. Moreover, lampalizumab showed an acceptable safety profile. A more substantial monthly treatment benefit of 44% reduction in geographic atrophy progression versus sham control was observed in a subgroup of patients who were complement factor I risk-allele carriers.